ResearchGate

See discussions, stats, and author profiles for this publication at: https://www.researchgate.net/publication/229958352

Ligand-Assisted Assembly Approach to Synthesize Large-Pore Ordered Mesoporous Titania with Thermally Stable and Crystalline Framework

ARTICLE *in* ADVANCED ENERGY MATERIALS · MARCH 2011

Impact Factor: 16.15 · DOI: 10.1002/aenm.201000004

CITATIONS
47

READS
54

10 AUTHORS, INCLUDING:

Yonghui Deng
Fudan University
101 PUBLICATIONS **5,065** CITATIONS
SEE PROFILE

Dong Gu
Max Planck Institute for Coal Research
78 PUBLICATIONS **4,133** CITATIONS
SEE PROFILE

Shutao Wang
ETH Zurich
10 PUBLICATIONS **415** CITATIONS
SEE PROFILE

Zhong-Sheng Wang
Fudan University
107 PUBLICATIONS **7,124** CITATIONS
SEE PROFILE

Available from: Shutao Wang
Retrieved on: 17 January 2016

Ligand-Assisted Assembly Approach to Synthesize Large-Pore Ordered Mesoporous Titania with Thermally Stable and Crystalline Framework

Junyong Zhang, Yonghui Deng, Dong Gu, Shutao Wang, Lan She, Renchao Che, Zhong-Sheng Wang, Bo Tu, Songhai Xie, and Dongyuan Zhao**

A novel ligand-assisted assembly approach is demonstrated for the synthesis of thermally stable and large-pore ordered mesoporous titanium dioxide with a highly crystalline framework by using diblock copolymer poly(ethylene oxide)-*b*-polystyrene (PEO-*b*-PS) as a template and titanium isopropoxide (TIPO) as a precursor. Small-angle X-ray scattering, X-ray diffraction (XRD), transmission electron microscopy (TEM), high-resolution scanning electron microscopy, and N_2-sorption measurements indicate that the obtained TiO_2 materials possess an ordered primary cubic mesostructure with large, uniform pore diameters of about 16.0 nm, and high Brunauer–Emmett–Teller surface areas of ~112 m^2 g^{-1}, as well as high thermal stability (~700 °C). High resolution TEM and wide-angle XRD measurements clearly illustrate the high crystallinity of the mesoporous titania with an anatase structure in the pore walls. It is worth mentioning that, in this process, in addition to tetrahydrofuran as a solvent, acetylacetone was employed as a coordination agent to avoid rapid hydrolysis of the titanium precursor. Additionally, stepped evaporation and heating processes were adopted to control the condensation rate and facilitate the assembly of the ordered mesostructure, and ensure the formation of fully polycrystalline anatase titania frameworks without collapse of the mesostructure. By employing the obtained mesoporous and crystallized TiO_2 as the photoanode in a dye-sensitized solar cell, a high power-conversion efficiency (5.45%) can be achieved in combination with the N719 dye, which shows that this mesoprous titania is a great potential candidate as a catalyst support for photonic-conversion applications.

1. Introduction

Titania and titania-based materials have stimulated considerable interest because of their promising applications for photoinduced electron transfer, as photoconductors, sensors, photocatalysts, and dye-sensitized solar cells (DSSCs), as well as in water purification.[1–9] Most of these applications are strongly dependent on the surface structure,[4] crystallization degree and large surface area of titania and titania-based materials.[9] Ordered mesoporous materials possess extraordinarily large surface areas and well-arranged channels or pores[10–12] that can greatly facilitate mass diffusion within frameworks. Much work has been done to synthesize ordered mesoporous titanias by using various strategies, such as the evaporation-induced self-assembly (EISA) method; however, most methods rely on the use of commercial Pluronic triblock copolymers like poly(ethylene oxide)-*b*-poly(propylene oxide)-*b*-poly(ethylene oxide), PEO_{20}-PPO_{70}-PEO_{20} (P123), and PEO_{106}-PPO_{70}-PEO_{106} (F127) as templates.[13–27] For instance, Yang et al.[13] synthesized ordered mesoporous titania by adopting Pluronic P123 as a template, $TiCl_4$ as a precursor, and ethanol as the solvent, by using the solvent EISA method. Tian et al.[17] developed an acid–base pair strategy for self-adjustment of the precursors hydrolysis rate, by using Pluronic F127 as a template. This conventional EISA approach to synthesize ordered mesoporous titania-based materials is very sensitive to preparation conditions, such as solvent purity, temperature, and relative humidity, which can affect the sol-gel process of titanium precursors and thus disruptthe synthesis.[24,25] Moreover, since conventional soft-templating synthesis processes involve the use of the commercial PEO-PPO-PEO triblock copolymers as templates, they usually lead to pore sizes smaller than 10 nm in the mesoporous titania due to the limitation of the chain length of the hydrophobic PPO segments. More importantly, during calcination for the removal of the template or post-treatment for crystallization, the framework inevitably undergoes intense reorganization, which results in shrinkage and even collapse of mesostructures.[13,28,29]

To overcome this problem, a nanocasting method based on ordered mesoporous silica or carbon as a hard template has been applied to synthesize various mesoporous titanias. However, the nanocasting method is costly, time-consuming, and laborious.[30–34] Recently, an efficient method[35] was reported

Dr. J. Y. Zhang, Dr. Y. H. Deng, D. Gu, S. T. Wang, Dr. L. She,
Prof. R. C. Che, Prof. Z.-S. Wang, Prof. B. Tu, S. H. Xie, Prof. D. Y. Zhao
Department of Chemistry
Shanghai Key Laboratory of Molecular Catalysis and Innovative Materials and Advanced Materials Laboratory
Fudan University
Shanghai 200433, P.R. China
E-mail: yhdeng@fudan.edu.cn; dyzhao@fudan.edu.cn;
Homepage: http://homepage.fudan.edu.cn/~dyzhao/

DOI: 10.1002/aenm.201000004

© 2011 WILEY-VCH Verlag GmbH & Co. KGaA, Weinheim

by Wiesner and co-workers, which gives direct access to mesoporous TiO_2 materials by using amorphous carbon derived from amphiphilic block-copolymer templates as a rigid support to maintain the mesostructure during the crystallization. However, due to the difficulty in controlling the hydrolysis and condensation of the titania precursors as well as the assembly of amphiphilic copolymer templates and precursors, the obtained mesoporous titania still has a partly disordered mesostructure. The synthesis of ordered and crystalline mesoporous titania materials with large pores is still a challenge.

Herein, we demonstrate a novel ligand-assisted assembly method for the synthesis of highly ordered and crystalline mesoporous titanias with uniform large pores using titanium isopropoxide (TIPO) as a precursor, diblock copolymer PEO-*b*-PS (PS=polystyrene) as a structure-directing agent, and tetrahydrofuran (THF) as a solvent. Notably, acetylacetone (AcAc) was employed as a coordination agent during the EISA process to retard the hydrolysis and condensation of the titania precursor by stabilizing the hydrolyzed Ti nanoentities by chelation, which makes the assembly process more controllable. By virtue of the supporting effect of carbon residues from the macromolecular template PEO-*b*-PS during carbonization in an inert atmosphere, ordered mesoporous titanias with primitive cubic mesostructure, highly crystallized anatase framework and large pore size (~16 nm), high Brunauer–Emmett–Teller (BET) surface areas of ~112 m^2 g^{-1}, and high thermal stability can be obtained. By using the synthesized large-pore mesoporous titania combined with N719 dye as a photoanode in a DSSC, a high power-conversion efficiency of 5.45% can be achieved.

2. Results and Discussion

2.1. Diblock-Copolymer Template

The amphiphilic diblock copolymer PEO-*b*-PS was prepared using a simple atom-transfer radical polymerization (ATRP) method.[36] Its chemical structure and composition were confirmed by Fourier-transform infrared (FTIR) spectroscopy (Supporting Information, Figure S1), gel permeation chromatography (GPC; Figure S2) and ^{1}H-NMR spectroscopy. GPC measurements show a polydispersity index (PDI) of 1.19, which indicates a narrow molecular weight distribution. The molecular weight was measured to be ~18000 g mol^{-1}, and the composition can be formulated as PEO_{125}-*b*-PS_{130}.

2.2. Ordered Mesoporous TiO_2 Templated From PEO-*b*-PS Diblock Copolymers

The as-made mesoporous PEO-*b*-PS/TiO_2 composites prepared by the ligand-assisted assembly method are homogeneously transparent yellow membranes, which is indicative of a well-assembled mesostructure without phase separation. The small angle X-ray scattering (SAXS) pattern (**Figure 1**a) of the as-made PEO-*b*-PS/TiO_2 composites clearly shows six scattering peaks at q values of 0.27, 0.53, 0.83, 1.11, 1.44, and 1.68 nm^{-1}. These well-resolved scatterings have the ratio of 1 : 2 : 3 : 4 : 5 : 6, and can be indexed as the 100, 200, 221/300, 400, 430/500, and 442/600 reflections of the primitive cubic mesostructure, respectively, according to the law of extinction. The result clearly indicates that a highly ordered cubic mesostructure is obtained via ligand-assisted assembly. The unit-cell parameter (a) is calculated to be as large as 23.2 nm. After the pyrolysis of PEO-*b*-PS/TiO_2 composites at 350 °C under high-purity N_2 for 2 h, the obtained powder (MPTi-350N) is gray in appearance, which implies that in situ carbonization of PEO_{125}-*b*-PS_{130} templates occurs in the mesochannels. The SAXS pattern (Figure 1b) of the obtained mesoporous titania MPTi-350N also displays three well-resolved scattering peaks, which suggest that the ordered cubic mesostructure is retained. The cell parameter (a) is calculated to be ~21.5 nm, smaller than that of the as-made composite, which suggests a structural shrinkage of ~7.3% (**Table 1**) due to the condensation of the titania framework and decomposition of templates.

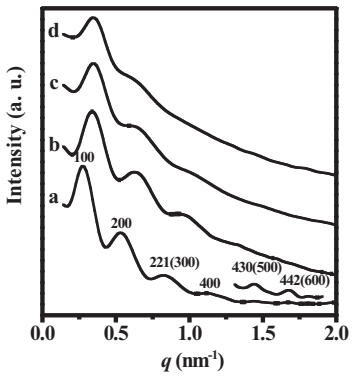

Figure 1. SAXS patterns of the ordered mesoporous titanias prepared by the ligand-assisted assembly method. a) As-made composite; b) MPTi-350N, c) MPTi-600N, and d) MPTi-600N-450A obtained after calcination at 350 °C or 600 °C in N_2, or 600 °C in N_2 followed by 450 °C in air, respectively.

After further pyrolysis under N_2 at 600 °C for the framework crystallization, the obtained mesoporous titania (MPTi-600N) is still gray, which reflects the presence of carbon residue. Similar

Table 1. Physicochemical properties of the ordered mesoporous TiO_2 obtained under various conditions.

Sample	d_{100} [nm]	a [nm]	D [nm]	S_{BET} [m^2 g^{-1}]	V_t [cm^3 g^{-1}]	V_{mi} [cm^3 g^{-1}]	W_t [nm]
As-made composite	23.2	23.2	–	–	–	–	–
MPTi-350N	21.5	21.5	16.1	79.5	0.18	0.005	5.4
MPTi-600N	20.0	20.0	16.0	112	0.21	0.002	4.0
MPTi-600N-450A	20.0	20.0	15.3	94.6	0.27	0	4.7

d-spacing values were calculated using the formula $d = 2\pi/q$, and the unit-cell parameters were calculated from the formula $a = d_{100}$. The wall thickness values were calculated from $W_t = a - D$, where a represents the cell parameter and D is the pore diameter.[37] The pore volumes and pore size distributions were calculated from the Broekoff–de Boer (BdB) sphere model.[38] S_{BET} is the total BET surface area. V_t and V_{mi} are the total pore volume and micropore volume, respectively.

© 2011 WILEY-VCH Verlag GmbH & Co. KGaA, Weinheim

to that of MPTi-350N, the SAXS pattern of the sample MPTi-600N shows three resolved scattering peaks, but the intensity is slightly lower (Figure 1c), due to the crystallization of the titania framework at high temperature. The cell parameter (*a*) is calculated to be ~20.0 nm, which is slightly less than that of MPTi-350N and indicates a minor shrinkage. The SAXS pattern of the sample MPTi-700N obtained by further calcination at 700 °C in N_2 shows one resolved scattering peak, confirming the high stability of the mesostructure (Figure S3). The high stability of the samples in N_2 is related to the supporting effect exerted by carbon residues in the mesochannels. When the sample MPTi-600N was further calcined in air at 450 °C for 2 h, a white powder (MPTi-600N-450A) was obtained, which implies that the supporting carbon residues are removed by combustion. The SAXS pattern of MPTi-600N-450A still shows two resolved peaks (Figure 1d), which suggest that the mesostructure is well preserved. However, direct calcination of the as-made PEO-*b*-PS/TiO_2 composite in air only yields porous titania with a collapsed mesostructure (Figure S4). This result suggests the carbon residues from the in situ carbonization of the PEO-*b*-PS template in the channels contribute to the preservation of mesostructure and therefore the two-step calcination strategy is indispensable for the formation of ordered mesoporous titania with a crystallized framework.

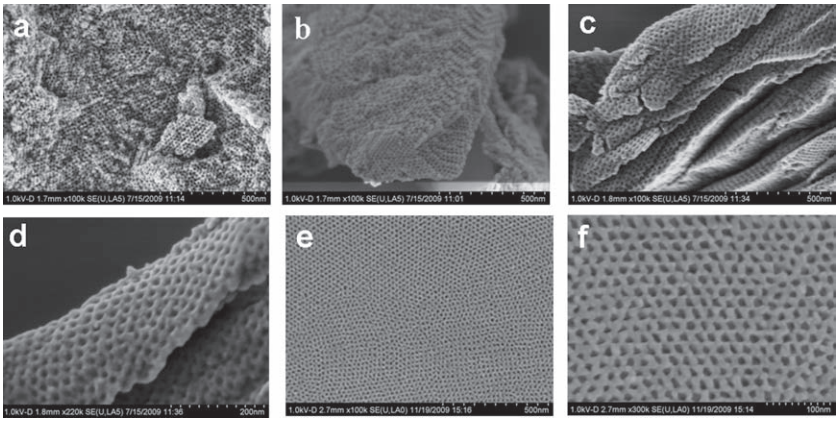

Figure 3. FESEM images of the ordered mesoporous titanias prepared by the ligand-assisted assembly method after calcination at 350 °C or 600 °C in N_2, or 600 °C in N_2 then 450 °C in air. a,b) MPTi-350N, c,d) MPTi-600N, e,f) MPTi-600N-450A.

Wide-angle X-ray diffraction (WAXRD) patterns of the mesoporous titania sample MPTi-350N show no diffraction peak, which indicates an amorphous feature (**Figure 2**a). The sample MPTi-600N after pyrolysis at 600 °C in N_2 (Figure 2b) displays seven well-resolved diffraction peaks, which can be indexed to the 101, 004, 200, 105/211, 204, 116/220, and 215 reflections of anatase [JPDF no. 21–1272]. This result suggests that the amorphous mesoporous titania can be converted into a highly crystallized phase by heating at 600 °C. Using the Scherrer equation, the crystallite size of the sample MPTi-600N is calculated to be ~9.1 nm. The sample MPTi-600N-450A, calcined at 450 °C in air, retains the anatase phase (Figure 2c), and the crystallite size increases to ~10.2 nm, revealing the further growth of crystalline grains in the framework. The X-ray diffraction (XRD) pattern of the sample MPTi-700N obtained after pyrolysis at 700 °C in N_2 for 3 h exhibits several diffraction peaks that correspond to mixed rutile and anatase phases (Figure S5); this suggests a transformation from the anatase to rutile phase when the calcination temperature increases. The Raman spectrum of MPTi-600N (Figure S6a) shows two bands around 1300 and 1600 cm^{-1}, which confirm the existence of the in situ formed amorphous carbon, and these two vibration bands do not feature in the spectrum of PTi-600N-450A (Figure S6b) that was obtained by further calcination at 450 °C in air, which implies a successful removal of carbon. The themogravimetry conducted in air shows a distinct weight loss of 4.5% around 310 °C–430 °C for MPTi-600N due to the removal of carbon residues, while almost no weight loss is detected for MPTi-600N-450A (Figure S7), which further confirms that the carbon residues are completely removed.

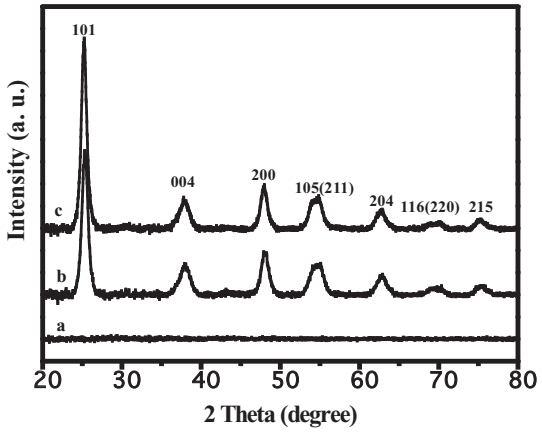

Figure 2. WAXRD patterns of the ordered mesoporous titanias: a) MPTi-350N, b) MPTi-600N and c) MPTi-600N-450A after being calcined at 350 °C or 600 °C in N_2, or 600 °C in N_2 followed by 450 °C in air, respectively.

Field-emission scanning electron microscopy (FESEM) images reveal that both MPTi-350N and MPTi-600N (**Figure 3**) exhibit highly ordered arrays of uniform spherical mesopores in whole particles, which suggests a long-range mesostructural regularity. The sample MPTi-600N displays better contrast in SEM images than does MPTi-350N, due to its higher crystallinity. After burning out the carbon residues at 450 °C in air, the ordered mesopore arrays are retained in MPTi-600N-450A, and the surface morphology becomes rougher because of the thermal annealing of frameworks in air and removal of carbon supporting (Figure 3e, 3f). SEM images of MPTi-700N annealed at 700 °C in N_2 (**Figure 4**) display spherical mesopores, but the regularity declines significantly, and many large TiO_2 crystal grains can be observed on the surface, which hints at a phase conversion from the anatase to rutile. Transmission electron microscopy (TEM) images further confirm the formation of ordered cubic mesoporous titania structure with large pores and crystallized walls. A high degree of periodicity over large domains viewed from the [100], [111], and [210] directions of a

© 2011 WILEY-VCH Verlag GmbH & Co. KGaA, Weinheim

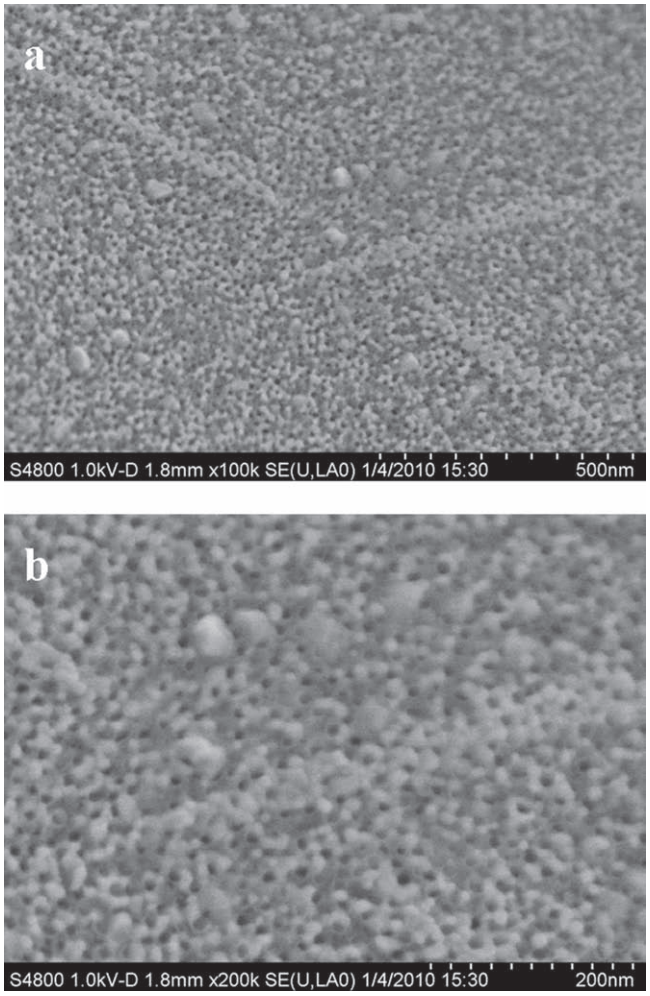

Figure 4. HRSEM images of the mesoporous titania sample MPTi-700N after pyrolysis at 700 °C in N_2 for 3 h, with magnification of a) x200 k and b) x300 k.

primitive cubic mesostructure is observed for MPTi-600N after pyrolysis at 600 °C in N_2, which is consistent with results from the SAXS analysis. The selected-area electron diffraction (SAED) shows a series of spotty diffraction pattern rings (**Figure 5**e) which corresponding to a polycrystalline anatase phase, and agree well with XRD results. Lattice fringes of the nanocrystals around the mesopores can be clearly observed in the high-resolution transmission electron microscopy (HRTEM) image (Figure 5d). The cell parameter is evaluated from TEM images to be ~20.0 nm, consistent with the value calculated from the SAXS pattern. The TEM image (Figure S8) of MPTi-600N-450A, obtained after removing the carbon residues by combustion at 450 °C in air, shows that the ordered cubic mesostructure is well retained, and regular arrays of spherical pore can be clearly observed over a large domain, further confirming an excellent thermal stability. To check the existence of residual carbon in the sample MPTi-600N, the gray power was immersed into concentrated sulfuric acid and heated to 100 °C for 12 h to remove the TiO_2 framework. The TEM image of the remaining black sample shows a hollow vesicle-like structure. Energy dispersive X-ray (EDX) measurements reveal that the vesicles contain only elemental carbon (Figure S9). These results suggest that amorphous carbon hollow spheres are formed in situ in the mesochannels during the carbonization in N_2, and these act as a rigid scaffold to support the mesostructural framework during the crystallization of titania at high temperature.

The nitrogen-sorption isotherm of the mesoporous titania MPTi-350N, obtained by pyrolysis at 350 °C in N_2, shows characteristic type IV curves with a sharp capillary condensation step in the relative pressure (P/P_0) of 0.78–0.90, which suggests uniform mesopores with large pore size (**Figure 6**A,a). Characteristic H_2-type hysteresis loops are observed at P/P_0 of ~0.42, which imply caged uniform mesopores with a small entrance size (<5.0 nm), similar to those observed in the previous report.[39] A narrow pore-size distribution at mean diameters as large as 16.1 nm is obtained from the BdB sphere model (Figure 6B,a). The wall thickness is calculated to be about 5.4 nm. The BET surface area is 79.5 $m^2\ g^{-1}$, and the total pore volume is 0.18 $cm^3\ g^{-1}$ (Table 1). MPTi-600N exhibits similar type IV isotherms to those of MPTi-350N, with a sharp capillary condensation at a slightly lower P/P_0 of 0.76–0.85, which suggests a decrease in pore size due to mesostructure shrinkage during crystallization at 600 °C (Figure 6A,b). The sample MPTi-600N has a uniform mesopore size of ~16 nm and wall thickness of 4.0 nm (Table 1), slightly smaller than that of MPTi-350N due to the framework shrinkage (Figure 6B,b). Moreover, the BET surface area and pore volume of MPTi-600N significantly increase over those of MPTi-350N, to 112 $m^2\ g^{-1}$ and 0.21 $cm^3\ g^{-1}$, respectively, which result from the further pyrolysis of carbonaceous species in mesopore channels (Table 1). Notably, further N_2-sorption isotherms of the sample MPTi-600N-450A obtained by further calcination at 450 °C in air (Figure 6A,c) show a capillary condensation step at a relative pressure of around 0.85 and H_1-type hysteresis loops with capillary evaporation occurring at ~0.7–0.8. This result indicates a uniform mesopore with a large pore opening. The mean mesopore size is ~15.3 nm and the pore wall thickness is ~4.7 nm. The window size is calculated to be about 9.0 nm, much larger than those of MPTi-350N and MPTi-600N (Table 1). This disparity probably results from the removal of the supporting carbon embedded in the spheres and windows during combustion in air, which thus leaves more voids. The BET surface area of MPTi-600N-450A is ~94.6 $m^2\ g^{-1}$ (Table 1), slightly lower than the values of its parent samples due to the contraction and the disappearance of micropores from the supporting carbon.

2.3. Formation of Mesostructures

In this work, a home-synthesized diblock copolymer PEO-*b*-PS was employed as a structure-directing agent. By using ligand-assisted assembly strategy, highly ordered and crystalline mesoporous TiO_2 materials with large pores and primitive cubic symmetry were obtained. Based on the aforementioned results, we propose a possible mechanism (**Scheme 1**) for the formation of such ordered mesoporous titanias with cubic structure and thermally stable crystallized frameworks. We believe that AcAc ligands can interact with the Ti ions of the precursor by coordination bonds, which significantly retard their hydrolysis

© 2011 WILEY-VCH Verlag GmbH & Co. KGaA, Weinheim

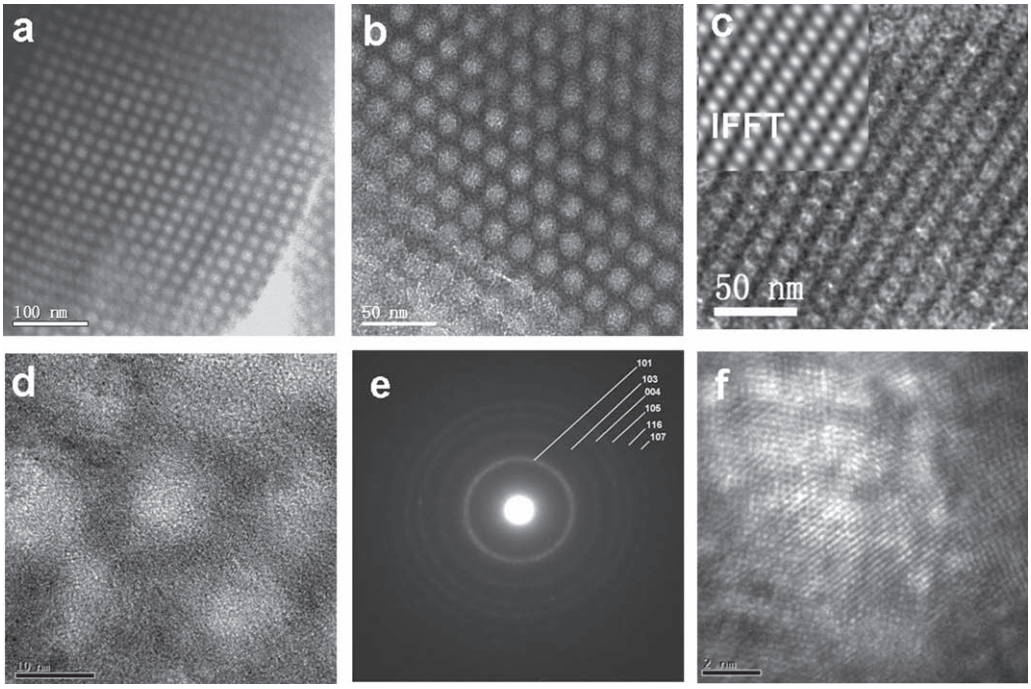

Figure 5. TEM images of the large-pore mesoporous titania MPTi-600N viewed from a) [100], b,d) [111], and c) [210] directions. HRTEM images (d,f) of ordered mesoporous titania MPTi-600N, e) is the corresponding SAED pattern from (c), exhibiting diffraction rings indexed to anatase phase. Insert in (c) shows the corresponding inverse Fourier diffractograms (IFFT).

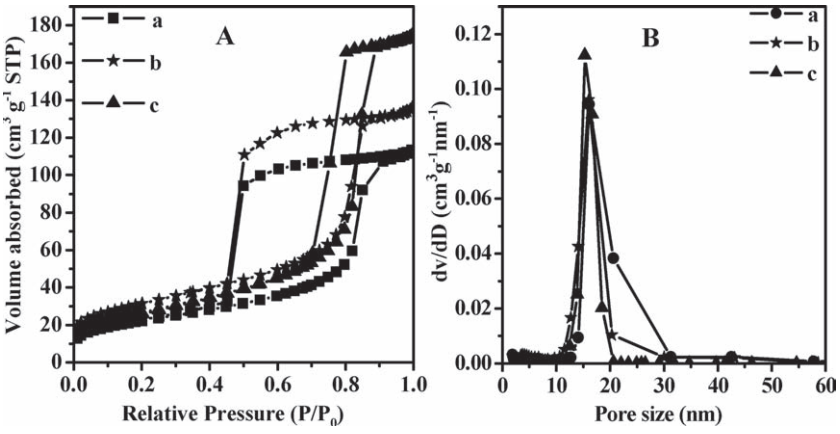

Figure 6. A) Nitrogen-sorption isotherms and B) pore-size distribution curves of the ordered mesoporous titania samples: a) MPTi-350N, b) MPTi-600N, and c) MPTi-600N-450A.

and condensation rate. The titania nanoentities are not liable to cross-link and can be stabilized over an extended period, which gives enough time for the structure-directing agents (the diblock copolymer) to assemble into the final phase. During the initial evaporation stage at 40 °C, the low-boiling point solvent, THF, is first removed, leaving more room and opportunity for the interaction of the PEO-*b*-PS molecules with titanium oligmers. At the annealing stage at 100 °C, AcAc molecules can be continuously evaporated, which induces the assembly of titania oligmers and PEO-*b*-PS templates, and the formation of the ordered mesostructure. The slow evaporation rate of AcAc not only helps to control the condensation rate of the titania species but also enhances the mobility of block copolymers for the organization of composite micelles into a primitive cubic mesostructure, driven by the lowering of surface energy. After the mesostructure is eventually fixed, the pyrolysis at 350 °C in N_2 can carbonize the diblock copolymer templates within mesochannels, producing a carbonaceous layer on the surface. Simultaneously, titania species are further cross-linked and condensed, which results in the formation of amorphous frameworks. Subsequent annealing at 600 °C in N_2 promotes the crystallization of the framework into anatase nanocrystals, while the ordered mesostructure is retained because of the protection of the carbon supports. The final combustion of the carbon at 450 °C in air gives ordered mesoporous titania with fully crystallized anatase pore walls. Additional evidence for the high crystallinity of the framework is provided by the HRTEM images (Figure 5f), which reveal that the main faces along the incident electron beam can be well indexed as [112] planes of anatase TiO_2. The results clearly demonstrate that almost all the mesopore walls are composed of anatase nanocrystals.

DSSC cells based on the ordered mesoporous titania (MPTi-600N-450A) obtained after removal of the carbon at 450 °C in air and also on the commercial nanoparticles P-25 as a standard were fabricated[40] and the performances were measured under the same conditions. As shown in **Figure 7**, under a simulated solar illumination (100 mW cm^{-2}), the P-25-based cell produces short-circuit photocurrent (J_{sc}) of 6.13 mA cm^{-2},

© 2011 WILEY-VCH Verlag GmbH & Co. KGaA, Weinheim

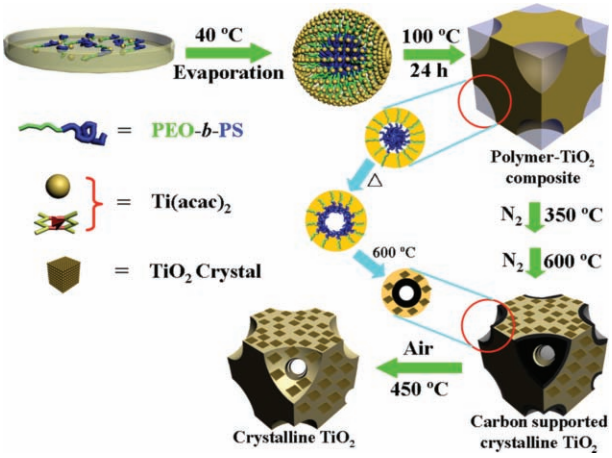

Scheme 1. Proposed formation process for the ordered and highly crystallivzed large-pore mesoporous titania materials with cubic structure from the ligand-assisted assembly method.

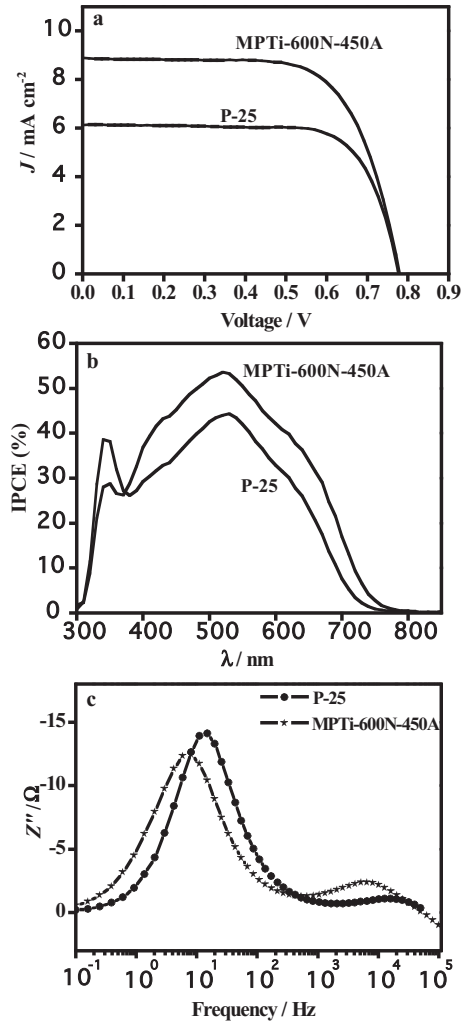

Figure 7. a) *J–V* curves for DSSCs based on P-25 and on the ordered mesoporous TiO_2 (MPTi-600N-450A) films with a thickness of ~11 μm. b) IPCE as a function of incident monochromatic wavelength. c) Bode plots of DSSCs under illumination with simulated solar light (100 mW cm^{-2}).

open-circuit photovoltage (V_{oc}) of 0.78 V, and fill factor (FF) of 0.72, which corresponds to a power-conversion efficiency of 3.44%, whereas the ordered mesoporous titania-based cell generates J_{sc} of 8.90 mA cm^{-2}, V_{oc} of 0.78 V, and FF of 0.68, which corresponds to a power-conversion efficiency of 4.72%. The ordered mesoporous titania shows higher photocurrent and power-conversion efficiency than the standard P-25 particles. Increasing the film thickness to 16 nm can increase the power-conversion efficiency to 5.45% with 9.32 mA cm^{-2} of J_{sc}, 0.78 V of V_{oc}, and 0.75 of FF, mainly due to the increased dye loading.

Figure 7b shows the incident monochromatic photon-to-electron conversion efficiency (IPCE) as a function of the wavelength of incident monochromatic light. It is evident that the mesoporous titania DSSC generates a higher IPCE in the wavelength range of 400–800 nm. The significant increase of IPCE in the visible region is responsible for the remarkable increase in J_{sc}, as shown in Figure 7a. IPCE or J_{sc} is determined by the light-harvesting efficiency (LHE), electron-injection yield, and charge-collection efficiency. As the electron-injection yield is unity for N719-sensitized titania, as confirmed by ultrafast transient absorption spectra,[41] LHE and charge-collection efficiency are the two key factors determining IPCE generation. To understand the difference of J_{sc} between the two kinds of DSSCs, the adsorbed amount of the dye was determined by UV-vis absorption spectroscopy for the dye-loaded films. The mesoporous titania film adsorbs more dye molecules than the P-25 film by 73% (Figure S10), which is consistent with the difference in BET surface area (79.5 and 49 m^2 g^{-1} for MPTi-600N-450A and P-25, respectively). Considering the increase with the film thickness, the absorbance for 11-μm films is estimated to be 1.03 and 1.77 for the mesoporous titania and P-25, respectively. The LHE of the mesoporous titania cell should be larger than that of P-25 by 8%, which cannot completely account for the 23% increase of the maximum IPCE. Based on the above analysis, the large difference in IPCE or J_{sc} may be attributed to the different charge-collection efficiency, which is related to the nature of titania.[42]

To understand the electron-transport properties of the photoelectrodes, the electron lifetime can be extracted from the electrochemical impedance spectra (EIS) measurements. Figure 7c shows the Bode plots of the DSSCs under one-sun illumination. The high-frequency peak corresponds to the charge-transfer behavior at the Pt/electrolyte interface, while the low-frequency peak is due to electron transfer at the TiO_2/dye/electrolyte interface. The electron lifetime (τ_n) can be calculated from the relation $\tau_n = 1/(2\pi f_m)$, where f_m is the frequency of the low-frequency peak in the Bode plot (Figure 7c). The electron lifetime of the mesoporous titania-based DSSC is 26 ms, which is 2.4 times that of the P-25. The ordered mesostructure may have fewer defects for charge recombination, which may yield longer electron lifetime than the P-25. As a consequence, higher IPCE and J_{sc} values are observed in the ordered mesoporous-titania-based DSSC. These results suggest that our ordered mesoporous TiO_2 is promising for applications in DSSCs. Although the J_{sc} value is lower than the value reported in the literature,[43] we believe that the performance could be improved significantly after enhancing the adsorbed dye amount by enlarging the pore entrance size.

© 2011 WILEY-VCH Verlag GmbH & Co. KGaA, Weinheim

3. Conclusions

In summary, we demonstrate a ligand-assisted assembly approach to successfully synthesize ordered mesoporous titania materials with a primitive cubic structure and highly crystalline anatase frameworks by using diblock copolymer PEO_{125}-*b*-PS_{130} as a template, TIPO as a titania source, THF as the solvent, and AcAc as a coordination agent. Two evaporation stages and two heating steps were adopted; the former favors the control of the titanium cross-link and assembly of ordered mesostructure, and the latter ensures the stabilization of mesostructure and formation of fully polycrystalline anatase framework with a size of ~11.2 nm. The obtained titania materials have a large uniform mesopore size (~16 nm), thick pore wall (~4 nm), and large surface area (~112 m^2 g^{-1}), as well as excellent thermal stability (up to 700 °C), which are unique features for applications in various fields such as photodegradation of pollutants, water splitting, etc. The obtained mesoporous TiO_2 films when used as a photoanode have a power-conversion efficiency of up to 5.45% in dye-sensitized solar cells. Additionally, since this method is simple and reproducible, and insensitive to synthesis conditions, it can be used as a versatile method for the synthesis of ordered mesoporous metal oxides, such as Al_2O_3.

4. Experimental Section

4.1. Chemicals

Monomethoxy poly(ethylene oxide) (PEO5000, molecular weight = 5000), 2-bromoisobutyryl bromide, and *N*,*N*′,*N*′,*N*′,*N*″-pentamethyldiethylenetriamine (PMDETA) were purchased from Acros Corp. Titanium isopropoxide [$Ti(OCH(CH_3)_2)_4$, TIPO] was obtained from Fluka. Tetrahydrofuran (THF), pyridine, styrene, ethylether, CuBr, petroleum ether (b.p. 60–90 °C), AcAc, and HCl (36 wt%) were purchased from Shanghai Chemical Corp. Styrene (St) was purified by filtrating through an Al_2O_3 column. *cis*-di(thiocyanato)-bis(2,2′-bipyridyl-4,4′-dicarboxylate) ruthenium (II), the so-called N719, was purchased from Solaronix SA (Switzerland). All other chemicals were used as received without further purification.

4.2. Preparation of PEO-b-PS Diblock Copolymer

The amphiphilic PEO_{125}-*b*-PS_{130} diblock copolymers were prepared through a simple ATRP method involving two steps. The first step was the synthesis of macroiniator PEO-Br. Monomethoxy PEO 5000 (10.0 g) was dissolved in THF (30 mL), and then 20 mL of pyridine were then added to obtain a homogeneous solution. The solution was placed in an ice-water bath, and 1.50 g (6.5 mmol) of 2-bromoisobutyrylbromide were added dropwise under stirring for 30 min. The resultant solution was further stirred at 30 °C overnight. After cooling to room temperature, cold ether (100 mL) was added to the solution. The white PEO-Br was precipitated from the reaction solution, washed with cold ether, and dried in vacuum. Then 5.0 g (1.0 mmol) of PEO-Br, 0.10 g (1.0 mmol) of CuCl, 0.173 g (1.0 mmol) of PMDETA, and 30.0 g (288 mmol) of styrene were added to an ampoule bottle. The bottle, containing reactants, was fully degassed with three freeze pump–thaw cycles and sealed under vacuum. It was subsequently immersed in a thermostated oil bath at 110 °C under stirring to allow polymerization of styrene. After reaction for 4 h, the system was cooled down to room temperature. The product was dissolved in 50 mL of THF and filtered through an Al_2O_3 column to remove the catalyst. Petroleum ether (200 mL) was poured into the solution to precipitate the PEO-*b*-PS diblock copolymer. The copolymer was then dried in vacuum.

4.3. Synthesis of Ordered Mesoporous Titanias

The ordered mesoporous titanias were prepared by using the diblock copolymer PEO-*b*-PS as a template and TIPO as a precursor. For a typical synthesis, the lab-made PEO-*b*-PS (0.10 g, 5.6×10^{-3} mmol) was dissolved in 5.0 mL (61.7 mmol) of THF, while 0.60 g (2.1 mmol) of TIPO was dissolved in 0.90 g (9 mmol) of AcAc. The above two solutions were mixed with stirring for 30 min at room temperature. Sequentially, 0.60 g of concentrated HCl (36 wt%) was added dropwise under vigorous stirring, followed by further stirring for 30 min. The obtained red-colored homogeneous solution was poured into petri dishes to evaporate the solvents at room temperature for 5 min, followed by sequential heating at 40 °C for 24 h and at 100 °C for another 24 h to completely remove solvents. Finally, the light-yellow membrane was scraped and crushed into powder which was denoted as as-made composite sample. To retain the mesostructure, the powder was first pyrolyzed in a tubular furnace under N_2 at 350–600 °C for 3 h, which resulted in a gray carbon-supported titania powder. White mesoporous TiO_2 products were obtained by further calcination of the carbon-supported titania powder in air at 450 °C for 2 h to burn out the carbon supports. The as-made samples and the obtained products pyrolyzed at 350, 600 °C in N_2, and 450 °C in air were assigned as MPTi-as-made, MPTi-350N, MPTi-600N, and MPTi-600N-450A, respectively.

4.4. Photovoltaic Measurements

Mesoporous TiO_2 films with thicknesses of 11 and 16 μm were fabricated on conductive glass (fluorine-doped SnO_2, 15 Ω/square, transmittance 85%, Asahi Co.) by using a doctor-blade technique and then sintered at 525 °C for 1 h with a rise rate of 10 °C min^{-1}. *cis*-Di(thiocyanato)-bis(2,2′-bipyridyl-4,4′-dicarboxylate) ruthenium (II), the so-called N719 (Solaronix SA), was used as a dye sensitizer to stain TiO_2 electrodes. Redox electrolyte used in this work contained 0.1 M LiI, 0.05 M I_2, 0.6 M 4-*tert*-butylpyridine, and 0.6 M 1,2-dimethyl-3-*n*-propyl-imidazolium iodide in dry acetonitrile. Dye sensitization of TiO_2, device assembly and encapsulation, and electrolyte injection to the inner space of the DSSCs were as in the literature method.[44]

The *J*–*V* characteristics were measured with a Keithley 2400 Source Meter under the illumination of AM1.5 simulated solar light coming from a solar simulator (Oriel-91193 equipped with a 1000 W Xe lamp and an AM1.5 filter). The light intensity was calibrated by using a reference Si solar cell (Oriel-91150). A black metal mask with aperture area of 0.2304 cm^2 was attached to the device surface to avoid stray light during the measurement. IPCE spectra were measured with an Oriel-74125 system (Oriel Instruments, USA), where the intensity of monochromatic light was measured with a Si detector (Oriel-71640). The EIS were measured on an electrochemical workstation (Zahner, Germany) under open-circuit. The EIS under illumination of simulated AM 1.5 solar light (100 mW cm^{-2}) were scanned in the frequency range of 0.1–100 kHz and at the ac amplitude of 10 mV.

4.5. Characterization and Measurements

XRD patterns were recorded with a Bruker D4 powder X-ray diffractometer using Cu Kα radiation (40 kV, 40 mA). SAXS measurements were taken on a Nanostar U system (Bruker, Germany) using Cu Kα radiation (40 kV, 35 mA). The *d*-spacing values were calculated by the formula $d = 2\pi/q$. The wall thickness was calculated from $W_t = a - D$, where a represents the cell parameter and D is the pore diameter calculated from the N_2-sorption

© 2011 WILEY-VCH Verlag GmbH & Co. KGaA, Weinheim

measurements. Thermogravimetric analysis (TGA) measurements for the diblock copolymer PEO_{125}-*b*-PS_{130} template and the mesoporous PEO-*b*-PS/TiO_2 composites (MPTi-as-made) were carried out by using a Mettler Toledo TGA-SDTA851 analyzer (Switzerland) from 25 °C to 800 °C under nitrogen with a heating rate of 5 °C min^{-1}. TEM images were conduced on a JEOL JEM-2100F (UHR) microscope (Japan) operated at 200 kV. The samples for TEM measurements were suspended in ethanol solution and supported onto a holey carbon film on a Cu grid. HRSEM images were taken using a field-emission Hitachi S-4800 (Japan) operated at 1.0 kV. Nitrogen-sorption isotherms were measured at 77 K with a Micromeritics Tristar 3000 analyzer (USA). Before measurements, the samples were degassed in vacuum at 200 °C for at least 6 h. The BET method was utilized to calculate the specific surface areas. By using the BdB sphere-model method, the pore volumes and pore-size distributions were calculated from the adsorption branches of isotherms, and the total pore volumes (V_t) were estimated from the adsorbed amount at a relative pressure P/P_0 of 0.992. The micropore volumes (V_m) and micropore surface areas (S_m) were calculated from the *V-t* plot method by using the equation V_m (cm^3) = 0.001547*I*, where *I* represents the *y* intercept in the *V-t* plots. The *t* values were calculated as a function of the relative pressure using the de Bore equation, t/Å = [13.99/(log (P_0/P) + 0.0340)]$^{1/2}$. FTIR spectra were collected on a Nicolet Fourier spectrophotometer (USA) using KBr pellets. GPC was performed on a LC-10ADvp gel permeation chromatographer (Shimadz, Japan) with refractive index detector and UV-vis detector (wavelength 190–950 nm, USA) using THF as an eluent (1.0 mL min^{-1}). GPC was calibrated with monodisperse polystyrene standards. Raman spectra were obtained with a Dilor LabRam-1B microscopic Raman spectrometer (France), using an He–Ne laser with an excitation wavelength of 632.8 nm.

Supporting Information

Supporting Information is available from the Wiley Online Library or from the author.

Acknowledgements

This work was supported by NSF of China (20821140537, 20871030, 20890123, 20971025, 21073040 and 90922004), State Key Basic Research Program of PRC (2009AA033701), Shanghai Leading Academic Discipline Project (B108), Shanghai Rising Star program (08QA14010), Shanghai Pujiang Program (09PJ1401300), and Shanghai Innovation Program of Science and Technology (10530705300). We greatly appreciate the financial support from from Delta Environmental & Educational Foundation (Taiwan) and Fudan Graduate Innovation Funds.

Received: October 19, 2010
Revised: November 26, 2010
Published online: January 25, 2011

[1] X. He, D. Antonelli, *Angew. Chem, Int. Ed.* **2001**, *41*, 214.
[2] A. Hagfeldt, M. Grätzel, *Chem. Rev.* **1995**, *95*, 49.
[3] J. Tang, Y. Y. Wu, E. W. McFarland, G. D. Stucky, *Chem. Commun.* **2004**, 1670.
[4] T. Kawahara, Y. Konishi, H. Tada, N. Tohge, J. Nishii, S. Ito, *Angew. Chem. Int. Ed.* **2002**, *41*, 2811.
[5] R. Asahi, T. Morikawa, T. Ohwaki, K. Aoki, Y. Taga, *Science* **2001**, *293*, 269.
[6] C. Lettmann, H. Hinrichs, W. F. Maier, *Angew. Chem. Int. Ed.* **2001**, *40*, 3160.
[7] U. Bach, D. Lupo, P. Comte, J. E. Moser, F. Weissortel, J. Salbeck, H. Spreitzer, M. Grätzel, *Nature* **1998**, *395*, 583.
[8] P. Prene, E. Lancelle-Beltran, C. Boscher, P. Belleville, P. Buvat, C. Sanchez, *Adv. Mater.* **2006**, *18*, 2579.
[9] M. Zukalova, A. Zukal, L. Kavan, M. K. Nazeeruddin, P. Liska, M. Grätzel, *Nano Lett.* **2005**, *5*, 1789.
[10] Y. Wan, H. F. Yang, D. Y. Zhao, *Acc. Chem. Res.* **2006**, *39*, 423.
[11] Y. Wan, Y. F. Shi, D. Y. Zhao, *Chem. Commun.* **2007**, 897.
[12] Y. Wan, D. Y. Zhao, *Chem. Rev.*, **2007**, *107*, 2821.
[13] P. D. Yang, D. Y. Zhao, D. I. Margolese, B. F. Chmelka, G. D. Stucky, *Nature* **1998**, *396*, 152.
[14] P. D. Yang, D. Y. Zhao, D. I. Margolese, B. F. Chmelka, G. D. Stucky, *Chem. Mater.* **1999**, *11*, 2813.
[15] M. H. Bartl, S. P. Puls, J. Tang, H. C. Lichtenegger, G. D. Stucky, *Angew. Chem. Int. Ed.* **2004**, *43*, 3037.
[16] P. C. A. Alberius, K. L. Frindell, R. C. Hayward, E. J. Kramer, G. D. Stucky, B. F. Chmelka, *Chem. Mater.* **2002**, *14*, 3284.
[17] B. Z. Tian, X. Y. Liu, B. Tu, C. Z. Yu, J. Fan, L. M. Wang, S. H. Xie, G. D. Stucky, D. Y. Zhao, *Nat. Mater.* **2003**, *2*, 159.
[18] B. Z. Tian, H. F. Yang, X. Y. Liu, S. H. Xie, C. Z. Yu, J. Fan, B. Tu, D. Y. Zhao, *Chem. Commun.* **2002**, 1824.
[19] X. Xu, B. Z. Tian, J. L. Kong, S. Zhang, B. H. Liu, D. Y. Zhao, *Adv. Mater.* **2003**, *15*, 1932.
[20] R. Liu, Y. Ren, Y. Shi, F. Zhang, L. Zhang, B. Tu, D. Zhao, *Chem. Mater.* **2008**, *20*, 1140.
[21] W. Dong, Y. Sun, C. W. Lee, W. Hua, X. Lu, Y. Shi, S. Zhang, J. Chen, D. Y. Zhao, *J. Am. Chem. Soc* . **2007**, *129*, 13894.
[22] T. Yu, Y. Deng, L. Wang, R. Liu, L. Zhang, B. Tu, D. Y. Zhao, *Adv. Mater.* **2007**, *19*, 2301.
[23] D. L. Li, H. S. Zhou, I. Honma, *Nat. Mater.* **2004**, *3*, 65.
[24] S. Y. Choi, M. Mamak, N. Coombs, N. Chopra, G. A. Ozin, *Adv. Funct. Mater.* **2004**, *14*, 335.
[25] E. L. Crepaldi, G. J. de A. A. Soler-Illia, D. Grosso, F. Cagnol, F. Ribot, C. Sanchez, *J. Am. Chem. Soc.* **2003**, *125*, 9770.
[26] D. Grosso, G. J. De A. A. Soler-Illia, F. Babonneau, C. Sanchez, P. A. Albouy, A. Brunet-Bruneau, A. R. Balkenende, *Adv. Mater.* **2001**, *13*, 1085.
[27] G. J. de A. A. Soler-Illia, A. Louis, C. Sanchez, *Chem. Mater.* **2002**, *14*, 750.
[28] H. S. Yun, K. Miyazawa, H. S. Zhou, I. Honma, M. Kuwabara, *Adv. Mater.* **2001**, *13*, 1377.
[29] F. Schüth, *Chem. Mater.* **2001**, *13*, 3184.
[30] A. H. Lu, F. Schüth, *Adv.Mater.* **2006**, *18*, 1793.
[31] F. Kleitz, S. H. Choi, R. Ryoo, *Chem. Commun.* **2003**, 2136.
[32] X. Lai, X. Li, W. Geng, J. Tu, J. Li, S. Qiu, *Angew. Chem. Int. Ed.* **2007**, *46*, 738.
[33] J. Roggenbuck, M. Tiemann, *J. Am. Chem. Soc.* **2005**, *127*, 1096.
[34] W.-C. Li, A.-H. Lu, C. Weidenthaler, F. Schüth, *Chem. Mater.* **2004**, *16*, 5676.
[35] J. Lee, O. M. Christopher, S. C. Warren, M. Kamperman, F. J. DiSalvo, U. Wiesner, *Nat. Mater.* **2008**, *7*, 222.
[36] Y. H. Deng, T. Yu, Y. Wan, Y. F. Shi, Y. Meng, D. Gu, L. J. Zhang, Y. Huang, C. Liu, X. J. Wu, D. Y. Zhao, *J. Am. Chem. Soc.* **2007**, *129*, 1690.
[37] P. I. Ravikovitch, A. V. Neimark, *Langmuir* **2002**, *18*, 1550.
[38] J. C. P. Broekhoff, J. H. deBoer, *J. Catal.* **1967**, *9*, 8.
[39] J. Y. Zhang, Y. Deng, J. Wei, Z. Sun, D. Gu, H. Bongard, C. Liu, H. Wu, B. Tu, F. Schüth, D. Y. Zhao, *Chem. Mater.* **2009**, *21*, 3996.
[40] B. O'Regan, M. Grätzel, *Nature* **1991**, *353*, 737.
[41] J. B. Ashbury, R. J. Ellingson, H. N. Ghosh, S. Ferrere, A. J. Nozik, T. Lian, *J. Phys. Chem. B* **1999**, *103*, 3110.
[42] N.-G. Park, J. van de Lagemaat, A. J. Frank, *J. Phys. Chem. B.* **2000**, *104*, 8989.
[43] Z.-S. Wang, H. Kawauchi, T. Kashima, H. Arakawa, *Coord. Chem. Rev.* **2004**, *248*, 1381.
[44] Z.-S. Wang, M. Yanagida, K. Sayama, H. Sugihara, *Chem. Mater.* **2006**, *18*, 2912.

© 2011 WILEY-VCH Verlag GmbH & Co. KGaA, Weinheim